A new physically realisable internal 1:1 resonance in the coupled pendulum-slosh system

H. Alemi Ardakani [†] [1], T.J. Bridges[‡], & M.R. Turner[‡]

[†] Department of Mathematics and Statistics, University of Exeter, Devon EX4 4QF, UK

[‡] School of Mathematics and Physics, University of Surrey, Guildford GU2 7XH, UK

Abstract. The problem of dynamic coupling between a rectangular container undergoing planar pendular oscillations and its interior potential fluid sloshing is studied. The Neumann boundary-value problem for the fluid motion inside the container is deduced from the Bateman–Luke variational principle. The governing integro-differential equation for the motion of the suspended container, from a single rigid pivoting rod, is the Euler-Lagrange equation for a forced pendulum. The fluid and rigid-body partial differential equations are linearised, and the characteristic equation for the natural and resonant frequencies of the coupled dynamical system are presented. It is found that internal $1:1$ resonances exist for an experimentally realistic setup, which has important physical implications. In addition, a new instability is found in the linearised coupled problem whereby instability occurs when the rod length is shorter than a critical length, and an explicit formula is given.

1 Introduction

The problems of fluid sloshing in a stationary or forced container, and dynamics of a rigid body with a liquid-filled cavity have been the subject of a great deal of research. The works by Moiseyev and Rumyantsev (1968), Ibrahim (2005), Faltinsen and Timokha (2009) and Lukovsky (2015), and references therein, highlight the theoretical, numerical and experimental problems in these areas. The aim in this paper is to study instability and internal $1:1$ resonances in the problem of dynamic coupling between a suspended container, undergoing planar pendular oscillations, and its interior inviscid and incompressible fluid sloshing.

The mathematical problem of instability of sloshing motion in a vessel undergoing pivoted oscillations is studied by Turner, Alemi Ardakani and Bridges (2015), hereafter TAAB (2015). This problem is generalised in the current paper and it is proved that *experimentally realistic* internal $1:1$ resonances can be observed in the coupled pendulum-sloshing system in the finite depth, which has important physical implications. At resonance, the uncoupled symmetric sloshing mode resonates exactly with an anti-symmetric sloshing mode joined with the pendulum motion. The internal resonances are important because at the linear level it is a mechanism for excitation of symmetric fluid mode coupling to the rigid body motion, and at the nonlinear level a $1:1$ resonance is a pathway for energy transfer between the fluid and rigid body, and can give rise to much more

[1]Email address for correspondence: h.alemi-ardakani@exeter.ac.uk; 12th December 2022

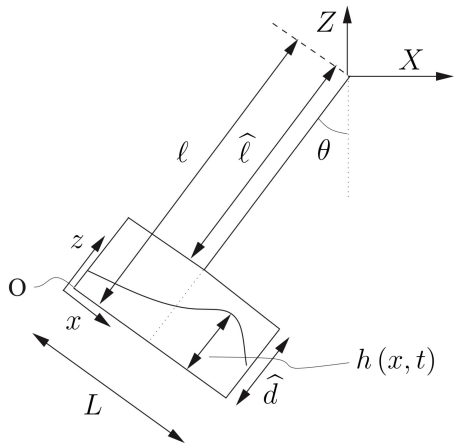

Figure 1: *Schematic showing a configuration of the coupled pendulum-slosh problem under consideration.*

dramatic fluid-body motion. Away from resonance, the anti-symmetric modes are the principal mechanism for coupling between the fluid and pendulum motion.

Consider a vessel with a rectangular cross-section of length L and height $\widehat{d}$ which is suspended by a rigid rod of length $\widehat{\ell}$ attached to the top of the vessel. A schematic is shown in Figure 1. The vessel is free to rotate in the vertical plane such that the rod makes an angle θ with the downward vertical. The perpendicular distance between the pivot point and the base of the vessel is $\ell = \widehat{d} + \widehat{\ell}$. The vessel is partially filled with an inviscid and incompressible fluid with constant density ρ. The fluid occupies the region $0 \leq z \leq h\,(x,t)$ with $0 \leq x \leq L$. The spatial (laboratory) frame has coordinates $\boldsymbol{X} = (X, Z)$ with origin at the pivot point, and the body frame has coordinates $\boldsymbol{x} = (x, z)$, which is attached to the moving vessel and used for the analysis of the interior fluid sloshing. The second body frame $\boldsymbol{x}_b = (x_b, z_b)$ is placed at the pivot point. The distance from the origin of the body frame $\boldsymbol{x}_b$, i.e. the pivot point, to the origin of the body frame $\boldsymbol{x}$ is denoted by $\boldsymbol{d} = (d_1, d_3)$, which is a constant vector. For our analysis in this paper it is $\boldsymbol{d} = (-L/2, -\ell)$.

Using the velocity potential theory, the Neumann boundary-value problem for the motion of the interior fluid sloshing can be obtained from the Bateman–Luke variational principle presented in Alemi Ardakani (2020). For our problem in this paper, we need the two-dimensional variant of the Bateman–Luke variational principle, which takes the form

$$\left.\begin{aligned}\delta\mathscr{L}\,(\Phi,h) = \delta\int_{t_1}^{t_2}\int_0^L\int_0^h -\Big(&\Phi_t + \tfrac{1}{2}\nabla\Phi\cdot\nabla\Phi + \Phi_x\dot{\theta}\,(z+d_3) - \Phi_z\dot{\theta}\,(x+d_1)\\ &+g\sin\theta\,(x+d_1) + g\cos\theta\,(z+d_3)\Big)\rho\,\mathrm{d}z\,\mathrm{d}x\,\mathrm{d}t = 0\,,\end{aligned}\right\} \tag{1.1}$$

subject to the endpoint conditions $\delta\Phi\,(\boldsymbol{x}, t_1) = \delta\Phi\,(\boldsymbol{x}, t_2) = 0$. The variational principle (1.1) gives the boundary-value problem for the interior potential fluid sloshing with the velocity field

$$\boldsymbol{u} = (u, w) = \Big(\Phi_x + \dot{\theta}\,(z+d_3)\,, \Phi_z - \dot{\theta}\,(x+d_1)\Big)\,, \tag{1.2}$$

where $\Phi\,(x,z)$ is the velocity potential. The field equation for the interior fluid becomes

$$\Delta\,\Phi = \Phi_{xx} + \Phi_{zz} = 0 \quad \text{in} \quad 0 \leq z \leq h\,(x,t)\,, \quad 0 \leq x \leq L\,. \tag{1.3}$$

Relative to the body frame $\boldsymbol{x}$, the rigid-wall boundary conditions are

$$\left.\begin{aligned} &\Phi_x = -\dot\theta\,(z+d_3) \quad \text{at} \quad x=0 \quad \text{and} \quad x=L\,, \\ &\Phi_z = \dot\theta\,(x+d_1) \quad \text{at} \quad z=0\,. \end{aligned}\right\} \tag{1.4}$$

The kinematic free surface boundary condition at $z=h\,(x,t)$ becomes

$$\Phi_z - \dot\theta\,(x+d_1) = h_t + \Big(\Phi_x + \dot\theta\,(h+d_3)\Big)\,h_x\,, \tag{1.5}$$

and the dynamic free surface boundary condition at $z=h\,(x,t)$ takes the form

$$\Phi_t + \tfrac{1}{2}\left(\Phi_x^2+\Phi_z^2\right) + \Phi_x\dot\theta\,(h+d_3) - \Phi_z\dot\theta\,(x+d_1) + g\sin\theta\,(x+d_1) + g\cos\theta\,(h+d_3) = 0\,. \tag{1.6}$$

The nonlinear integro-differential equation governing the motion of the suspended container, with interior potential fluid sloshing, undergoing pendular oscillations can be obtained from the equation (54) of Alemi Ardakani (2020) which takes the form

$$\left\{\begin{aligned} &\int_0^L\int_0^{h(x,t)} \Big(\dot\theta\,(x+d_1)\,\Phi_x + \dot\theta\,(z+d_3)\,\Phi_z + (x+d_1)\,\Phi_{zt} - (z+d_3)\,\Phi_{xt} \\ &\qquad\qquad + \left(\Phi_{xz}\,(x+d_1) - \Phi_{xx}\,(z+d_3)\right)\Big(\Phi_x + \dot\theta\,(z+d_3)\Big) \\ &\qquad\qquad + \left(\Phi_{zz}\,(x+d_1) - \Phi_{xz}\,(z+d_3)\right)\Big(\Phi_z - \dot\theta\,(x+d_1)\Big) \\ &\qquad\qquad + g\Big(\,(x+d_1)\cos\theta - (z+d_3)\sin\theta\Big)\Big)\,\rho\,\mathrm{d}z\,\mathrm{d}x \\ &+ m_v\left(\overline{x}_v^2+\overline{z}_v^2\right)\ddot\theta + m_v g\,(\overline{x}_v\cos\theta - \overline{z}_v\sin\theta) = 0\,, \end{aligned}\right. \tag{1.7}$$

where m_v is the mass of the dry container, $\overline{\boldsymbol{x}}_v = (\overline{x}_v, \overline{z}_v)$ is the centre of mass of the dry container relative to the body frame $\boldsymbol{x}_b$ placed at the pivot point.

In TAAB (2015) the centre of mass of the dry container is fixed at the centre of the base of the container. By introducing a new dimensionless variable $\lambda = \overline{z}_v/L$, the analytical results of TAAB (2015) can be extended to more general configurations. In particular, (a) the characteristic equations for the natural frequencies of the coupled pendulum-slosh system in finite depth and in the shallow water limit are extended; (b) exact formulae are derived for the instability threshold in the coupled system; and (c) a quadratic equation is found which leads to identification of the existence of internal $1:1$ resonances for experimentally realistic setups in the case of finite depth.

The outline of the paper is as follows. In §2 the forced nonlinear pendulum equation (1.7) for the rigid body motion, and the Neumann boundary-value problem (1.3), (1.4), (1.5), and (1.6) for the interior potential fluid motion are linearised about the state of quiescent fluid. Moreover, a characteristic equation is derived for the natural frequency of the coupled pendulum-slosh system. In §3 the instability condition of TAAB (2015) for the coupled pendulum-slosh oscillations is generalised. It is found that instability occurs in the linear coupled system if the rod length is shorter than a critical length, which depends on (a) the length of the container, (b) the initial fluid height at rest, (c) the ratio of the fluid and rigid body masses, and (d) the vertical coordinate of the centre of mass of the dry rigid body relative to the pivot point. The shallow water limit of the characteristic equation is presented in §4. In §5 a quadratic equation is derived, in finite depth and in the shallow water limit, for internal $1:1$ resonances in the coupled system. Numerical evaluations of the characteristic equation and results at $1:1$ resonance are presented in §6. The paper ends with concluding remarks in §7.

2 The characteristic equation for the linearised coupled pendulum-slosh system

To derive the characteristic function for the natural frequencies of the coupled (pendular rigid body motion + interior potential fluid sloshing) system, we linearise the governing equations about a state of quiescent fluid where $\Phi = -g\,(h_0 + d_3)\,t$, $h = h_0$, and $\theta = 0$ where the initial fluid height h_0 is a constant. Express $\Phi\,(x, z, t)$, $h\,(x, t)$, and $\theta\,(t)$ as time-periodic functions with frequency ω,

$$\Phi\,(x, z, t) = -g\,(h_0 + d_3)\,t + \widehat{\Phi}\,(x, z)\sin\omega t\,, \quad h\,(x, t) = h_0 + \widehat{h}\,(x)\cos\omega t\,, \quad \theta\,(t) = \widehat{\theta}\cos\omega t\,, \tag{2.1}$$

where $|\widehat{\Phi}|$, $|\widehat{h}|$, $|\widehat{\theta}| \ll 1$. Substituting these expressions into the Neumann boundary-value problem (1.3), (1.4), (1.5), and (1.6) for the fluid motion and retaining only linear terms leads to the following boundary-value problem for $\widehat{\Phi}$, $\widehat{h}$, and $\widehat{\theta}$:

$$\left.\begin{aligned}
&\widehat{\Phi}_{xx} + \widehat{\Phi}_{zz} = 0 \quad \text{in} \quad 0 \le z \le h_0\,, \quad 0 \le x \le L\,,\\
&\widehat{\Phi}_x = \widehat{\theta}\omega\,(z + d_3) \quad \text{at} \quad x = 0, L \quad \text{and} \quad \widehat{\Phi}_z = -\widehat{\theta}\omega\,(x + d_1) \quad \text{at} \quad z = 0\,,\\
&\widehat{\Phi}_z = -\widehat{h}\omega - \widehat{\theta}\omega\,(x + d_1) \quad \text{at} \quad z = h_0\,,\\
&\widehat{\Phi}\omega + g\widehat{h} + g\widehat{\theta}\,(x + d_1) = 0 \quad \text{at} \quad z = h_0\,.
\end{aligned}\right\} \tag{2.2}$$

Substituting (2.1) into the forced pendulum equation (1.7) for the rigid-body motion, setting $d_1 = -L/2$, $d_3 = -\ell$, $\overline{x}_v = 0$, the mass of the interior fluid $m_f = \rho h_0 L$, and retaining only linear terms gives

$$\left\{\begin{aligned}
&\left(m_v\overline{z}_v^2\omega^2 + m_v g\overline{z}_v + m_f g\left(\tfrac{1}{2}h_0 - \ell\right)\right)\widehat{\theta} - \int_0^L \rho g\widehat{h}\Big|^{z=h_0}\left(x - \tfrac{1}{2}L\right)\mathrm{d}x\\
&+ \int_0^L\int_0^{h_0}\left((z - \ell)\,\widehat{\Phi}_x - \left(x - \tfrac{1}{2}L\right)\widehat{\Phi}_z\right)\omega\rho\,\mathrm{d}z\,\mathrm{d}x = 0\,.
\end{aligned}\right. \tag{2.3}$$

We can eliminate $\widehat{h}(x)$ from the dynamic and kinematic free surface boundary conditions in (2.2) to get a single free surface boundary condition in terms of $\widehat{\Phi}$ and $\widehat{\theta}$ as

$$\widehat{\Phi}_z - \frac{\omega^2}{g}\,\widehat{\Phi} = 0 \quad \text{at} \quad z = h_0\,. \tag{2.4}$$

Substituting for $\widehat{h}$ from the kinematic free surface boundary condition in (2.2) with $d_1 = -L/2$ into (2.3) modifies the rigid body equation to

$$\left\{\begin{aligned}
&-\left(m_v\overline{z}_v^2\omega^2 + m_v g\overline{z}_v + m_f g\left(\tfrac{1}{2}h_0 - \ell\right) + \frac{1}{12}\rho g L^3\right)\widehat{\theta} - \int_0^L \frac{\rho g}{\omega}\widehat{\Phi}_z\Big|^{z=h_0}\left(x - \tfrac{1}{2}L\right)\mathrm{d}x\\
&= \int_o^L\int_0^{h_0}\left((z - \ell)\,\widehat{\Phi}_x - \left(x - \tfrac{1}{2}L\right)\widehat{\Phi}_z\right)\omega\rho\,\mathrm{d}z\,\mathrm{d}x\,.
\end{aligned}\right. \tag{2.5}$$

In TAAB (2015) the centre of mass of the dry rigid body is fixed at $\overline{\boldsymbol{x}}_v = (\overline{x}_v, \overline{z}_v) = (0, d_3) = (0, -\ell)$, which is the centre of the base of the rigid body. In this paper, the centre of mass of the dry rigid body is placed at $\overline{\boldsymbol{x}}_v = (0, \overline{z}_v)$ where $\overline{z}_v$ is any point along

the centre line. This leads to the generalisation of the analytical results of TAAB (2015) and proves that internal $1:1$ resonances can be observed in the coupled system in the finite depth for experimentally realistic parameters.

Now, the strategy for solving the boundary-value problem is to transform $\widehat{\Phi}(x,z)$ so that the inhomogeneous boundary conditions at $x=0,L$ in (2.2) are moved to $z=h_0$. Then a cosine expansion in the $x-$direction can be used (Alemi Ardakani *et al.* 2012). Let

$$\widehat{\Phi}(x,z)=\widehat{\theta}\omega\left(x-\tfrac{1}{2}L\right)(z-\ell)+\widehat{\phi}(x,z)\,. \tag{2.6}$$

The function $\widehat{\phi}(x,z)$ then satisfies the Laplace equation and the following boundary conditions

$$\begin{cases}\widehat{\phi}_x=0 \quad \text{at} \quad x=0,L\,,\\ \widehat{\phi}_z=-2\widehat{\theta}\omega\left(x-\tfrac{1}{2}L\right) \quad \text{at} \quad z=0\,,\\ \widehat{\phi}_z-\dfrac{\omega^2}{g}\,\widehat{\phi}=-\widehat{\theta}\omega\left(x-\tfrac{1}{2}L\right)+\dfrac{\omega^3}{g}\widehat{\theta}\left(x-\tfrac{1}{2}L\right)(h_0-\ell) \quad \text{at} \quad z=h_0\,.\end{cases} \tag{2.7}$$

Substituting the general form for $\widehat{\phi}(x,z)$ in (2.6) into the coupling equation (2.5) for $\widehat{\theta}$ gives

$$\begin{cases}-\left(m_v g\overline{z}_v+m_f g\left(\tfrac{1}{2}h_0-\ell\right)+\dfrac{1}{6}\rho g L^3\right)\widehat{\theta}-\left(m_v\overline{z}_v^2+m_f\left(\dfrac{1}{3}h_0^2+\ell^2-\ell h_0-\dfrac{1}{12}L^2\right)\right)\omega^2\widehat{\theta}\\ -\displaystyle\int_0^L\frac{\rho g}{\omega}\left(x-\tfrac{1}{2}L\right)\widehat{\phi}_z\Big|^{z=h_0}\mathrm{d}x=\int_0^L\int_0^{h_0}\left((z-\ell)\,\widehat{\phi}_x-\left(x-\tfrac{1}{2}L\right)\widehat{\phi}_z\right)\omega\rho\,\mathrm{d}z\,\mathrm{d}x\,.\end{cases} \tag{2.8}$$

The right-hand side of the free surface boundary condition in (2.7) can be written as a cosine expansion (Alemi Ardakani *et al.* 2012) by noting that

$$x-\frac{L}{2}=-\frac{4}{L}\sum_{n=0}^{\infty}\frac{1}{\alpha_n^2}\cos\alpha_n x \quad \text{with} \quad \alpha_n=(2n+1)\,\frac{\pi}{L}\,, \tag{2.9}$$

where α_n represents the wavenumbers for the anti-symmetric sloshing modes. Thus the Laplace equation together with the boundary conditions (2.7) form a boundary value problem for $\widehat{\phi}$ and $\widehat{\theta}$.

The general solution to Laplace's equation which satisfies the rigid-wall boundary conditions at $x=0,L$ in (2.7) is

$$\left.\begin{aligned}\widehat{\phi}(x,z) \;=\;& A+Bz+\sum_{n=1}^{\infty}\left(b_n\cosh\beta_n z+c_n\sinh\beta_n z\right)\cos\beta_n x\\ &+\sum_{n=0}^{\infty}\left(a_n\cosh\alpha_n z+e_n\sinh\alpha_n z\right)\cos\alpha_n x\,,\end{aligned}\right\} \tag{2.10}$$

where $\beta_n=2n\pi/L$ corresponds to the symmetric sloshing modes and A, B, a_n, b_n, c_n, and e_n are constants to be determined. Satisfying the bottom boundary condition in (2.7) leads to

$$B=0\,,\quad c_n=0\,,\quad e_n=\frac{8\omega\widehat{\theta}}{L\alpha_n^3}\,, \tag{2.11}$$

using (2.9), so $\widehat{\phi}\,(x,z)$ takes the form

$$\widehat{\phi}\,(x,z) = A + \sum_{n=1}^{\infty} b_n \cosh\beta_n z \cos\beta_n x + \sum_{n=0}^{\infty}\left(a_n \cosh\alpha_n z + \frac{8\omega\widehat{\theta}}{L\alpha_n^3}\sinh\alpha_n z\right)\cos\alpha_n x\,. \tag{2.12}$$

Substituting (2.12) into the free surface boundary condition in (2.7), using (2.9), and equating coefficients of the cosine terms leads to $A = 0$ and

$$\left\{\begin{array}{l} \displaystyle\sum_{n=1}^{\infty}\left(\beta_n \tanh\beta_n h_0 - \frac{\omega^2}{g}\right) b_n \cos\beta_n x = 0\,, \\ \displaystyle\sum_{n=0}^{\infty}\left(\alpha_n \tanh\alpha_n h_0 - \frac{\omega^2}{g}\right) a_n \cos\alpha_n x = \sum_{n=0}^{\infty}\left(\frac{8\omega^3}{gL\alpha_n^3}\tanh\alpha_n h_0 - \frac{8\omega}{L\alpha_n^2}\right. \\ \qquad\qquad\qquad\qquad \left. + \dfrac{4\omega g - 4\omega^3\,(h_0-\ell)}{gL\alpha_n^2\cosh\alpha_n h_0}\right)\widehat{\theta}\cos\alpha_n x\,. \end{array}\right. \tag{2.13}$$

Setting $T_n = \tanh\alpha_n h_0$, $\widehat{T}_n = \tanh\beta_n h_0$, and $C_n = \cosh\alpha_n h_0$ the conditions (2.13) are simplified to

$$\left.\begin{array}{l} \left(\beta_n \widehat{T}_n - \dfrac{\omega^2}{g}\right) b_n = 0\,, \\ \left(\alpha_n T_n - \dfrac{\omega^2}{g}\right) a_n = \left(\dfrac{8\omega^3}{gL\alpha_n^3}T_n - \dfrac{8\omega}{L\alpha_n^2} + \dfrac{4\omega g - 4\omega^3\,(h_0-\ell)}{gL\alpha_n^2 C_n}\right)\widehat{\theta}\,. \end{array}\right\} \tag{2.14}$$

These are true for each n.

2.1 The characteristic function

The characteristic function for the coupled pendulum-slosh system is found by substituting $\widehat{\phi}$ into the forced pendulum equation (2.8). This requires the evaluation of the following two integrals

$$\left.\begin{array}{l} \displaystyle\int_0^L\int_0^{h_0}\left((z-\ell)\,\widehat{\phi}_x - \left(x - \tfrac{1}{2}L\right)\widehat{\phi}_z\right)\omega\rho\,\mathrm{d}z\,\mathrm{d}x = \sum_{n=0}^{\infty}\left(-2\rho\omega\frac{a_n}{\alpha_n}\,(h_0-\ell)\,S_n\right. \\ \left. -\dfrac{16\rho\omega^2\widehat{\theta}}{L\alpha_n^4}\big(\,(h_0-\ell)\,C_n + \ell\big) + 4\rho\omega\frac{a_n}{\alpha_n^2}\big(C_n - 1\big) + \frac{32\rho\omega^2\widehat{\theta}}{L\alpha_n^5}S_n\right), \end{array}\right\} \tag{2.15}$$

and

$$\int_0^L \frac{\rho g}{\omega}\left(x - \tfrac{1}{2}L\right)\widehat{\phi}_z\,(x,h_0)\,\mathrm{d}x = \sum_{n=0}^{\infty} -2\frac{\rho g}{\omega}\left(\frac{a_n}{\alpha_n}S_n + \frac{8\omega\widehat{\theta}}{L\alpha_n^4}C_n\right)\,, \tag{2.16}$$

where $S_n = \sinh\alpha_n h_0$. Now, substituting (2.15) and (2.16) into the forced pendulum equation (2.8) gives

$$\Theta\widehat{\theta} + \sum_{n=0}^{\infty}\left(-2\rho\left(\frac{g}{\omega} + \omega\,(h_0-\ell)\right)\frac{a_n}{\alpha_n}S_n + 4\rho\omega\,(C_n-1)\,\frac{a_n}{\alpha_n^2}\right) = 0\,, \tag{2.17}$$

where

$$\left.\begin{aligned}\Theta &= m_v\overline{z}_v^2\omega^2 + m_f\left(\frac{1}{3}h_0^2+\ell^2-\ell h_0-\frac{1}{12}L^2\right)\omega^2 + m_f g\left(\tfrac{1}{2}h_0-\ell\right)+m_v g\overline{z}_v\\ &\quad+\frac{1}{6}\rho g L^3+\sum_{n=0}^{\infty}\left(-\frac{16\rho g}{L\alpha_n^4}C_n+\frac{32\rho\omega^2}{L\alpha_n^5}S_n-\frac{16\rho\omega^2}{L\alpha_n^4}\left(\left(h_0-\ell\right)C_n+\ell\right)\right).\end{aligned}\right\} \tag{2.18}$$

The two equations in (2.14) and equation (2.17) provide three equations for the unknowns $\widehat{\theta}$, $a_0, a_1, \cdots$, and $b_1, b_2, \cdots$. The first equation in (2.14) is homogeneous, diagonal and decouples from the other equations. Its characteristic function is

$$P(\omega)=\prod_{n=1}^{\infty}\left(g\beta_n\widehat{T}_n-\omega^2\right)=0\,. \tag{2.19}$$

The full characteristic equation is

$$\Delta(\omega)=P(\omega)\,D(\omega)=0\,. \tag{2.20}$$

The symmetric modes, satisfying $P(\omega)=0$, do not appear in the coupling equation (2.17). As a consequence, the eigenvectors associated with the b_n modes are linearly independent from any of the eigenvectors of the other modes — a fact which is important for the internal $1:1$ resonance (Alemi Ardakani *et al.* 2012). It remains to derive the characteristic function $D(\omega)$ for non-resonant *strictly coupled* dynamics. It is this characteristic equation which was first studied by Cooker (1994) for sloshing frequencies in a suspended container but in the shallow water limit. Assume $\widehat{\theta}\neq 0$. Then the second equation in (2.14) can be solved for a_n and substituted into (2.12)

$$\left.\begin{aligned}\widehat{\phi}(x,z)=\sum_{n=1}^{\infty}b_n\cosh\beta_n z\cos\beta_n x+\sum_{n=0}^{\infty}\Bigg[&\frac{4\omega\widehat{\theta}}{L\alpha_n^2\left(g\alpha_n T_n-\omega^2\right)}\left(2\omega^2\frac{T_n}{\alpha_n}-2g+\frac{g}{C_n}\right.\\ &\left.-\frac{\omega^2\left(h_0-\ell\right)}{C_n}\right)\cosh\alpha_n z+\frac{8}{L\alpha_n^3}\widehat{\theta}\omega\sinh\alpha_n z\Bigg]\cos\alpha_n x\,.\end{aligned}\right\} \tag{2.21}$$

The second equation of (2.14) and the pendulum equation (2.17) can be expressed in matrix form as

$$\begin{bmatrix} g\alpha_0T_0-\omega^2 & 0 & 0 & \dots & 0 & 0 & -\chi_0\\ 0 & g\alpha_1T_1-\omega^2 & 0 & \dots & 0 & 0 & -\chi_1\\ \vdots & \vdots & \ddots & \vdots & \vdots & \vdots & \\ 0 & 0 & 0 & \dots & g\alpha_{n-1}T_{n-1}-\omega^2 & 0 & -\chi_{n-1}\\ 0 & 0 & 0 & \dots & 0 & g\alpha_nT_n-\omega^2 & -\chi_n\\ \Gamma\dfrac{S_0}{\alpha_0}+\Lambda_0 & \Gamma\dfrac{S_1}{\alpha_1}+\Lambda_1 & \Gamma\dfrac{S_2}{\alpha_2}+\Lambda_2 & \dots & \Gamma\dfrac{S_{n-1}}{\alpha_{n-1}}+\Lambda_{n-1} & \Gamma\dfrac{S_n}{\alpha_n}+\Lambda_n & \Theta \end{bmatrix}\begin{bmatrix} a_0\\ a_1\\ \vdots\\ a_{n-1}\\ a_n\\ \widehat{\theta}\end{bmatrix}=\mathbf{0}\,, \tag{2.22}$$

where

$$\begin{aligned}\Gamma &= -2\rho\omega\left(h_0-\ell\right)-\frac{2\rho g}{\omega}\,,\quad \Lambda_n=4\rho\omega\frac{C_n-1}{\alpha_n^2}\,,\\ \chi_n &= \frac{8\omega^3}{L\alpha_n^3}T_n-\frac{8\omega g}{L\alpha_n^2}+\frac{4\omega g-4\omega^3\left(h_0-\ell\right)}{L\alpha_n^2C_n}\,.\end{aligned}$$

The homogeneous equation (2.22) has a solution if and only if the determinant of the coefficient matrix vanishes. Using an infinite determinant expansion, this condition provides the characteristic function $D(\omega) = 0$. This strategy is used by Frandsen (2005) and TAAB (2015) to derive a product formula for the characteristic equation.

Alternatively, set $b_n = 0$ for all n. Then, substitution of a_n given by

$$a_n = \frac{4\omega\widehat{\theta}}{C_n L\alpha_n^2\left(g\alpha_n T_n - \omega^2\right)}\left(\frac{2C_n}{\alpha_n}\left(\omega^2 T_n - g\alpha_n\right) + g - \omega^2\left(h_0 - \ell\right)\right),$$

into (2.15) and (2.16) gives respectively

$$\left.\begin{aligned}&\int_0^L\int_0^{h_0}\left(\left(z-\ell\right)\widehat{\phi}_x - \left(x-\tfrac{1}{2}L\right)\widehat{\phi}_z\right)\omega\rho\,\mathrm{d}z\,\mathrm{d}x\\ &= \sum_{n=0}^{\infty}\left[\frac{-8\rho\omega^2\widehat{\theta}}{L\alpha_n^4\left(g\alpha_n T_n - \omega^2\right)}\left(g\alpha_n T_n\left(h_0+\ell\right) - \omega^2\alpha_n T_n\left(h_0-\ell\right)^2\right.\right.\\ &\qquad\left.\left.+2\omega^2\left(h_0-\ell\right)\left(1-\frac{2}{C_n}\right) + 6g\left(\frac{1}{C_n}-1\right) + \frac{4\omega^2 T_n}{\alpha_n} - 2\omega^2\ell\right)\right],\end{aligned}\right\}$$

and

$$\int_0^L \frac{\rho g}{\omega}\left(x-\tfrac{1}{2}L\right)\widehat{\phi}_z\left(x,h_0\right)\mathrm{d}x = \sum_{n=0}^{\infty}\left[\frac{-8\rho g\widehat{\theta}}{L\alpha_n^3\left(g\alpha_n T_n - \omega^2\right)}\left(\frac{-2\omega^2}{\alpha_n C_n} + T_n\left(g - \omega^2\left(h_0-\ell\right)\right)\right)\right].$$

Hence, the coupling equation (2.8) for $\widehat{\theta}$ gives an explicit expression for $D(\omega) = 0$ with

$$\left.\begin{aligned}D(\omega) &= m_v g\overline{z}_v + m_f g\left(\tfrac{1}{2}h_0 - \ell\right) + m_v\overline{z}_v^2\omega^2 + m_f\left(\frac{1}{3}h_0^2 + \ell^2 - \ell h_0 - \frac{1}{12}L^2\right)\omega^2\\ &+\frac{1}{6}\rho g L^3 - \sum_{n=0}^{\infty}\left[\frac{8\rho g}{L\alpha_n^3\left(g\alpha_n T_n - \omega^2\right)}\left(\frac{-2\omega^2}{\alpha_n C_n} + T_n\left(g + 2\omega^2\ell\right) - \frac{\omega^4}{g}T_n\left(h_0-\ell\right)^2\right.\right.\\ &\qquad\left.\left.+\frac{2\omega^4}{g\alpha_n}\left(h_0-\ell\right)\left(1-\frac{2}{C_n}\right) + \frac{6\omega^2}{\alpha_n}\left(\frac{1}{C_n}-1\right) + \frac{4\omega^4}{g}\frac{T_n}{\alpha_n^2} - \frac{2\omega^4\ell}{g\alpha_n}\right)\right].\end{aligned}\right\} \tag{2.23}$$

Exact solutions of this equation are impossible, but this explicit form can be used for numerical computation of the frequencies.

2.2 Non-dimensional characteristic function

The characteristic equation (2.20) can be expressed in terms of the non-dimensional parameters first proposed by Cooker (1994)

$$R = \frac{m_v}{m_f} \quad \text{and} \quad G = \frac{L\left(1+R\right)}{4\delta\ell} \quad \text{with} \quad \delta = \frac{h_0}{L}, \tag{2.24}$$

and an additional non-dimensional parameter associated with the vertical coordinate of the centre of mass of the dry container defined by

$$\lambda = \frac{\overline{z}_v}{L}. \tag{2.25}$$

Set the dimensionless natural frequency

$$s = \frac{L}{2}\frac{\omega}{\sqrt{gh_0}}\,. \tag{2.26}$$

Let

$$\begin{cases} \gamma_n = (2n+1)\,\pi = \alpha_n L\,, \quad \widehat{\gamma}_n = 2n\pi = \beta_n L\,, \quad \dfrac{\ell}{L} = \dfrac{1+R}{4\delta G}\,, \quad \omega^2 = \dfrac{4}{L}\delta g s^2\,, \\ T_n = \tanh\delta\gamma_n\,, \quad \widehat{T}_n = \tanh\delta\widehat{\gamma}_n\,, \quad S_n = \sinh\delta\gamma_n\,, \quad C_n = \cosh\delta\gamma_n\,. \end{cases} \tag{2.27}$$

This leads to the non-dimensional characteristic function for the dimensionless frequency s:

$$\Delta(s) \;\; = \;\; P(s)\,D(s) = 0\,, \tag{2.28}$$

where

$$\left.\begin{aligned} D(s) = {} & \left(R\lambda^2 - \frac{1}{12} + \frac{1}{3}\delta^2 + \left(\frac{1}{4\delta}\frac{1+R}{G}\right)^2 - \frac{1+R}{4G}\right)s^2 + \frac{1}{8} - \frac{1}{16\delta^2}\frac{1+R}{G} + \frac{1}{4\delta}R\lambda \\ & + \frac{1}{24\delta^2} - \sum_{n=0}^{\infty}\left[\frac{2}{\gamma_n^3\left(\gamma_n T_n - 4\delta s^2\right)}\left(\frac{16s^2}{\delta\gamma_n C_n} + \frac{T_n}{\delta^2}\left(1 + \frac{2(1+R)}{G}s^2\right)\right.\right. \\ & \qquad -16s^4 T_n\left(\delta - \frac{1}{4\delta}\frac{1+R}{G}\right)^2 + \frac{32s^4}{\gamma_n}\left(\delta - \frac{1}{4\delta}\frac{1+R}{G}\right)\left(1 - \frac{2}{C_n}\right) \\ & \qquad \left.\left. -\frac{24s^2}{\delta\gamma_n} + \frac{64s^4}{\gamma_n^2}T_n - \frac{8s^4}{\delta\gamma_n}\frac{1+R}{G}\right)\right]\,, \end{aligned}\right\} \tag{2.29}$$

and

$$P(s) = \prod_{n=1}^{\infty}\left(\widehat{\gamma}_n\widehat{T}_n - 4\delta s^2\right) \quad \text{or} \quad P(s) = \prod_{n=1}^{\infty}\left(s^2 - n^2\pi^2\frac{\tanh(2n\pi\delta)}{2n\pi\delta}\right)\,. \tag{2.30}$$

The characteristic function can be solved numerically for those complex roots s which have positive real part, for a given parameter set (G, R, δ, λ).

3 The instability condition in the coupled system

The characteristic function (2.28) exhibits both real (stable) and complex (unstable) solutions for the non-dimensional frequency s. The symmetric modes which are solutions to $P(s) = 0$ have solutions

$$s = \sqrt{\frac{\widehat{\gamma}_n\widehat{T}_n}{4\delta}}\,. \tag{3.1}$$

Due to the implicit form of $D(s)$ in (2.29) there is no analytical solution for the roots of the anti-symmetric modes. However, we can search for the roots of $D(s)$ numerically. The real roots of $D(s) = 0$ are found by plotting $D(s)$ for a fixed set of parameters (G, R, δ, λ) and calculating the values where this function crosses the real axis.

To find the complex roots of the characteristic function, it is noted that $D(s)$ in (2.29) is an even function of s, hence (2.29) can be solved for s^2, and when this quantity is negative the purely imaginary roots are found. The unstable solutions are restricted to a

particular region of the parameter space (G, R, δ, λ), which can be determined by solving (2.29) at $s^2 = 0$, which is the point at which instability occurs in the characteristic function. The result of this calculation gives a neutral stability contour in parameter space which separates the stable and unstable solutions. By setting $s = 0$ in (2.29) it can be shown that the neutral stability contour is analytically given by

$$\frac{1}{8} - \frac{1}{16\delta^2}\frac{1+R}{G} + \frac{1}{4\delta}R\lambda + \frac{1}{24}\frac{1}{\delta^2} - \sum_{n=0}^{\infty}\frac{2}{\delta^2}\frac{1}{\gamma_n^4} = 0\,. \tag{3.2}$$

Using the identity

$$\sum_{n=0}^{\infty}\frac{1}{\gamma_n^4} = \frac{1}{96}\,, \tag{3.3}$$

the expression (3.2) for the neutral stability condition reduces to

$$G = \frac{3\,(1+R)}{6\delta^2 + 12\delta R\lambda + 1}\,. \tag{3.4}$$

In TAAB (2015) the centre of mass of the dry rigid body is fixed at the centre of the base of the body. This means if we set $\overline{z}_v = -\ell$, which gives $\lambda = -\ell/L = -\,(1+R)\,/4\delta G$, then (3.2) recovers the equation (3.21) of TAAB (2015). From (3.4) one concludes that there is an instability in the coupled pendulum-slosh system if

$$\ell < \frac{1}{2}h_0 + \frac{1}{12}\frac{L^2}{h_0} + LR\lambda\,. \tag{3.5}$$

If we set $\overline{z}_v = -\ell$, then (3.5) recovers the instability condition (1.1) of TAAB (2015). Hence, the expression (3.5) is the extended form of the instability condition derived in TAAB (2015) with $\overline{x}_v = 0$ and $\overline{z}_v$ along the centre line passing through the pivot point and the centre of the base of the rigid body.

If we substitute $\overline{z}_v = -\mu\ell$ with μ a non-negative real number $\mu \in \mathbb{R}_{\geq 0}$, i.e. when the centre of mass of the dry container is placed at the pivot point ($\mu = 0$) or below the pivot point ($\mu \in \mathbb{R}_{>0}$) along the centre line, then the extended neutral stability condition (3.4) for the coupled pendulum-slosh system reduces to

$$G = \frac{3\,(1+R)\,(1+\mu R)}{1+6\delta^2}\,, \tag{3.6}$$

and the generalised instability condition (3.5) takes the form

$$\ell\,(1+\mu R) < \frac{1}{2}h_0 + \frac{1}{12}\frac{L^2}{h_0}\,. \tag{3.7}$$

Furthermore, if we substitute $\overline{z}_v = +\mu\ell$ with μ a positive real number $\mu \in \mathbb{R}_{>0}$, i.e. when the centre of mass of the dry container is placed above the pivot point along the centre line, then the neutral stability condition (3.4) for the coupled pendulum-slosh system reduces to

$$G = \frac{3\,(1+R)\,(1-\mu R)}{1+6\delta^2}\,, \tag{3.8}$$

and the generalised instability condition (3.5) takes the form

$$\ell\,(1-\mu R) < \frac{1}{2}h_0 + \frac{1}{12}\frac{L^2}{h_0}\,. \tag{3.9}$$

The expressions (3.7) and (3.9) are the extended forms of the instability condition derived in TAAB (2015) (see equation (1.1) in TAAB (2015)).

4 Shallow water limit of the characteristic function

The shallow water limit $\Delta^{\mathsf{SW}}(s) = 0$ of the characteristic function (2.28) can be calculated by letting $\delta \to 0$. Setting $\overline{z}_v = -\mu\ell$ in (2.29) with $\mu \in \mathbb{R}_{\geq 0}$, i.e. when the centre of mass of the dry container is placed at the pivot point or below the pivot point along the centre line, and noting that $T_n = \tanh(\gamma_n \delta) \to \gamma_n \delta$ as $\delta \to 0$ for any fixed n, using the identity (3.3), and interchanging the sum and limit gives the following expression for the shallow water limit of the characteristic function $D^{\mathsf{SW}}(s)$:

$$\left.\begin{aligned} D^{\mathsf{SW}}(s) &= \frac{1}{16}\frac{(1+R)^2(1+\mu^2 R)}{G^2}s^2 - \frac{1}{16}\frac{(1+R)(1+\mu R)}{G} + \frac{1}{24} \\ &- \sum_{n=0}^{\infty}\left[\frac{2}{\gamma_n^3(\gamma_n^2 - 4s^2)}\left(\frac{-8s^2}{\gamma_n} - \gamma_n\left(\frac{1+R}{G}\right)^2 s^4 + \gamma_n\left(1 + \frac{2(1+R)}{G}s^2\right)\right)\right]. \end{aligned}\right\} \tag{4.1}$$

To simplify further, two key identities are needed,

$$\sum_{n=0}^{\infty}\frac{1}{\gamma_n^2} = \frac{1}{8} \quad \text{and} \quad \tan(s) = 8s\sum_{n=0}^{\infty}\frac{1}{\gamma_n^2 - 4s^2}\,. \tag{4.2}$$

Now,

$$\frac{4}{\gamma_n^2}\frac{1}{(\gamma_n^2 - 4s^2)} = -\frac{1}{s^2}\frac{1}{\gamma_n^2} + \frac{1}{s^2}\frac{1}{\gamma_n^2 - 4s^2}\,, \tag{4.3}$$

and so $D^{\mathsf{SW}}(s)$ reduces to

$$\left\{\begin{aligned} D^{\mathsf{SW}}(s) &= \frac{(1+R)^2(1+\mu^2 R)}{G^2}s^2 - \frac{(1+R)(1+\mu R)}{G} \\ &\quad + \left(\frac{-1}{s^2} - \left(\frac{1+R}{G}\right)^2 s^2 + \frac{2(1+R)}{G}\right)\left(1 - \frac{\tan(s)}{s}\right). \end{aligned}\right. \tag{4.4}$$

To deduce the shallow water limit of $P(s)$ in (2.30), note that $\widehat{T}_n = \tanh(\widehat{\gamma}_n\delta) \to \widehat{\gamma}_n\delta$ as $\delta \to 0$ for any fixed n, and so

$$P^{\mathsf{SW}}(s) = \prod_{n=1}^{\infty}\left(\widehat{\gamma}_n^2 - 4s^2\right) = 0\,. \tag{4.5}$$

The characteristic function (4.5) can be replaced with

$$P^{\mathsf{SW}}(s) = \sin(s)\,, \tag{4.6}$$

because the roots of (4.5) occur at $s = n\pi$ which correspond to the roots of (4.6). Therefore the shallow water limit of the characteristic function (2.28) can be written as

$$\left.\begin{aligned} \Delta^{\mathsf{SW}}(s) &= P^{\mathsf{SW}}(s)\,D^{\mathsf{SW}}(s) \\ &= \sin(s)\left[\frac{(1+R)^2(1+\mu^2 R)}{G^2}s^2 - \frac{(1+R)(1+\mu R)}{G}\right. \\ &\quad \left. + \left(\frac{-1}{s^2} - \left(\frac{1+R}{G}\right)^2 s^2 + \frac{2(1+R)}{G}\right)\left(1 - \frac{\tan(s)}{s}\right)\right] = 0\,. \end{aligned}\right\} \tag{4.7}$$

Using a similar argument it can be proved that the shallow water limit of the characteristic function (2.28) when $\overline{z}_v = +\mu\ell$ in (2.29) with $\mu \in \mathbb{R}_{>0}$, i.e. when the centre of mass of the dry container is placed above the pivot point along the centre line, is

$$\left.\begin{aligned} \Delta^{\mathsf{SW}}(s) &= P^{\mathsf{SW}}(s)\, D^{\mathsf{SW}}(s) \\ &= \sin(s)\left[\frac{(1+R)^2(1+\mu^2 R)}{G^2}s^2 - \frac{(1+R)(1-\mu R)}{G}\right. \\ &\quad \left. + \left(\frac{-1}{s^2} - \left(\frac{1+R}{G}\right)^2 s^2 + \frac{2(1+R)}{G}\right)\left(1 - \frac{\tan(s)}{s}\right)\right] = 0\,. \end{aligned}\right\} \tag{4.8}$$

In the shallow water limit the unstable solutions are restricted to a particular region of the parameter space (G, R, μ). By setting $s = 0$ in (4.1) it can be shown that the shallow water neutral stability contour is analytically given by

$$G = 3(1+R)(1+\mu R)\,, \tag{4.9}$$

when the centre of mass of the dry container is placed at or below the pivot point, i.e. $\overline{z}_v = -\mu\ell$ with $\mu \in \mathbb{R}_{\geq 0}$. The instability contour (4.9) can be recovered from (3.6) by taking its limit as $\delta \to 0$. Hence, in terms of dimensional variables there is an instability in the system, in the limit of shallow water, if

$$\ell(1+\mu R) < \frac{1}{12}\frac{L^2}{h_0}\,. \tag{4.10}$$

Similarly, if the centre of mass of the dry container is placed above the pivot point, i.e. $\overline{z}_v = +\mu\ell$ with $\mu \in \mathbb{R}_{>0}$, the shallow water neutral stability contour is analytically given by

$$G = 3(1+R)(1-\mu R)\,. \tag{4.11}$$

This means there is an instability in the coupled shallow water system if

$$\ell(1-\mu R) < \frac{1}{12}\frac{L^2}{h_0}\,. \tag{4.12}$$

5 Experimentally realistic internal 1:1 resonances

The aim in this section is to generalise the resonance condition derived in TAAB (2015), and identify the existence of internal $1:1$ resonances in the coupled pendulum-slosh system in the finite depth for an *experimentally realistic* parameters G and R. The coupled system contains an internal $1:1$ resonance in finite depth where both symmetric and anti-symmetric modes have the same frequency. This occurs when the two factors of the characteristic function in (2.28) vanish simultaneously (Alemi Ardakani *et al.* 2012)

$$P(s) = 0 \quad \text{and} \quad D(s) = 0\,. \tag{5.1}$$

Setting the first factor to zero amounts to choosing a symmetric fluid mode; that is, for some $m \in \mathbb{N}$, $b_m \neq 0$ and $b_n = 0$ for all $n \neq m$, and

$$s_m = m\pi\sqrt{\frac{\tanh(2m\pi\delta)}{2m\pi\delta}}\,, \quad m = 1, 2, 3, \ldots\,. \tag{5.2}$$

At this value of s, for a $1:1$ resonance between the pendulum motion and the symmetric mode to exist the second term in the characteristic function must satisfy $D\left(s_m\right)=0$, which from (2.29) leads to the following quadratic equation for $G\left(R,\delta,\mu\right)$ with $\lambda=\mp\mu\ell/L$, $\mu\in\mathbb{R}$ ($-\mu$ when the centre of mass of the dry container is below the pivot point and $+\mu$ when the centre of mass of the dry container is above the pivot point):

$$\left.\begin{aligned}&\left(-\frac{1}{12}s_m^2+\frac{1}{3}\delta^2 s_m^2+\frac{1}{8}+\frac{1}{24\delta^2}-\sigma_1^{m,n}\right)G^2\\&+\left(-\frac{1}{4}\left(1+R\right)s_m^2-\frac{1}{16\delta^2}\left(1+R\right)\left(1\pm\mu R\right)-\sigma_2^{m,n}\right)G\\&+\frac{1}{16\delta^2}\left(1+R\right)^2\left(1+\mu^2R\right)s_m^2+\sigma_3^{m,n}=0\,,\end{aligned}\right\}\tag{5.3}$$

where

$$\left\{\begin{aligned}\sigma_1^{m,n}&=\sum_{n=0}^{\infty}\left[\frac{2}{\gamma_n^3\left(\gamma_nT_n-4\delta s_m^2\right)}\left(\frac{16s_m^2}{\delta\gamma_nC_n}+\frac{T_n}{\delta^2}-16s_m^4\delta^2T_n+\frac{32\delta s_m^4}{\gamma_n}\left(1-\frac{2}{C_n}\right)\right.\right.\\&\qquad\left.\left.-\frac{24s_m^2}{\delta\gamma_n}+\frac{64s_m^4}{\gamma_n^2}T_n\right)\right],\\\sigma_2^{m,n}&=\sum_{n=0}^{\infty}\left[\frac{2}{\gamma_n^3\left(\gamma_nT_n-4\delta s_m^2\right)}\left(\frac{2}{\delta^2}\left(1+R\right)s_m^2T_n+8s_m^4\left(1+R\right)T_n\right.\right.\\&\qquad\left.\left.+\frac{16s_m^4}{\delta\gamma_n}\left(1+R\right)\left(\frac{1}{C_n}-1\right)\right)\right],\\\sigma_3^{m,n}&=\sum_{n=0}^{\infty}\left[\frac{2T_ns_m^4}{\delta^2\gamma_n^3\left(\gamma_nT_n-4\delta s_m^2\right)}\left(1+R\right)^2\right].\end{aligned}\right.\tag{5.4}$$

Note that in order to determine whether or not a $1:1$ resonance is possible, the roots of the quadratic equation (5.3) should satisfy the stability condition

$$0<G<\frac{3\left(1+R\right)\left(1\pm\mu R\right)}{1+6\delta^2}\,.\tag{5.5}$$

The numerical experiments in §6 show that the quadratic equation (5.3), with the centre of mass of the dry rigid body placed below or above the pivot point along the centre line, leads to experimentally realistic values of G for $1:1$ resonances in the finite depth.

Similarly, in the shallow water limit, setting the first factor $P^{\mathsf{SW}}\left(s\right)$ in (4.7) and (4.8) to zero leads to the position of the $1:1$ resonance at

$$s_m=m\pi\,,\quad m\in\mathbb{N}\,.\tag{5.6}$$

Therefore, from $D^{\mathsf{SW}}\left(s\right)=0$ in (4.7) and (4.8) it can be inferred that

$$-G^2+\left(1+R\right)\left(1\mp\mu R\right)s_m^2G+\left(1+R\right)^2\mu^2Rs_m^4=0\,,\tag{5.7}$$

which has solutions

$$G=\tfrac{1}{2}\left(1+R\right)s_m^2\left(1\mp\mu R\pm\sqrt{\left(1\mp\mu R\right)^2+4\mu^2R}\right)\,,\tag{5.8}$$

or

$$G=\frac{1}{2}\left(1+R\right)m^2\pi^2\left(1\mp\mu R\pm\sqrt{\left(1\mp\mu R\right)^2+4\mu^2R}\right)\,,\tag{5.9}$$

where only the solutions with $G > 0$ are applicable. The quadratic equation (5.7) for G, at the internal $1:1$ resonance in the shallow water limit, is the generalised form of the quadratic equation derived in TAAB (2015). If we set $\mu = 1$ with $\overline{z}_v = -\ell$, i.e. the centre of mass of the dry rigid body is fixed at the centre of the base of the rigid body, then the solutions (5.8) recover the given results in TAAB (2015):

$$G = (1+R)\, m^2\pi^2 \quad \text{and} \quad G = -R\,(1+R)\, m^2\pi^2\,, \tag{5.10}$$

the second of which can be ignored as we consider only $G > 0$. In this case the internal $1:1$ resonance positions for the pendulum-slosh system occur at larger values of G for the same mass ratios $R = m_v/m_f$. Therefore, in TAAB (2015) it is concluded that the $1:1$ resonance is unlikely to be observed for an experimentally realistic setup.

Remarkably, in the current paper it is discovered that by placing the centre of mass of the dry rigid body above $\overline{z}_v = -\ell$ along the centre line, the new resonance equation (5.3) in the finite depth leads to experimentally realistic values of G for internal $1:1$ resonances, which has important physical implications. Details are given in §6 below.

6 Numerical evaluation of the characteristic equation and discussion of results

Numerical evaluations of the characteristic function in the finite depth, and results at $1:1$ resonance are presented in this section.

6.1 Results away from 1:1 resonance

First, the neutral stability contour (3.6), when the centre of mass of the dry container is placed below the point of suspension, with $\mu = 0.1$ and $\overline{z}_v = -0.1\ell$ relative to the pivot point, is shown in the (R, G) parameter space on the left in Figure 2 for different values of $\delta = 0.05, 0.2, 0.5$ and 0.8. Above this contour the solutions are unstable, while below the contour the solutions are stable. We only consider numerical results for $G > 0$, which corresponds to $\ell > 0$, which means the pivot point is above the bottom of the container. In terms of dimensional variables this says that there is an instability in the coupled system if (3.7) is satisfied. The consequence of (3.7) is that there is an instability in the system as the length of the rigid rod about which the container is pivoting tends to zero. The neutral stability contour (3.6), with $\mu = 0.6$ and $\overline{z}_v = -0.6\ell$ relative to the origin of the body frame placed at the pivot point, is illustrated in the (R, G)-plane on the right in Figure 2 for $\delta = 0.05, 0.2, 0.5$ and 0.8.

The neutral stability contour (3.8) in the (R, G) parameter space, when the centre of mass of the dry container is placed above the point of suspension, with $\mu = 0.2$, i.e. $\overline{z}_v = +0.2\ell$ relative to the origin of the body frame placed at the pivot point, and $\mu = 0.4$, i.e. $\overline{z}_v = +0.4\ell$ relative to the pivot point, are shown respectively on the left and on the right in Figure 3 for different values of $\delta = 0.05, 0.2, 0.5$ and 0.8. Above this contour the solutions are unstable, while below the contour the solutions are stable.

The roots of the characteristic equation $D(s) = 0$ give the dimensionless natural frequencies of the coupled motion. The simplest approach to finding the real roots is to plot $D(s)$ in (2.29) as a function of s. The approximate values can then be refined if necessary using Newton's method. First, substitute $\lambda = \mp\mu\ell/L$ with $\mu \in \mathbb{R}_{\geq 0}$, i.e. when

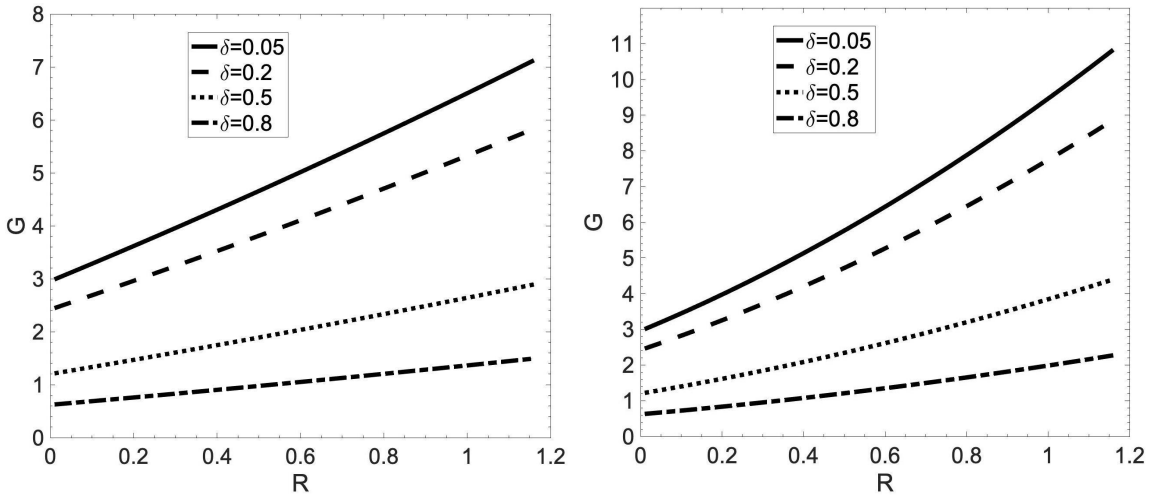

Figure 2: *On the left, plot of the neutral stability contour (3.6) in the* (R, G)*-plane with* $\mu = 0.1$ *and* $\overline{z}_v = -0.1\ell$ *for* $\delta = 0.05, 0.2, 0.5$ *and* 0.8*. On the right, plot of the neutral stability contour (3.6) in the* (R, G)*-plane with* $\mu = 0.6$ *and* $\overline{z}_v = -0.6\ell$ *for* $\delta = 0.05, 0.2, 0.5$ *and* 0.8*. Above the contour the solutions are unstable, while below the contour the solutions are stable.*

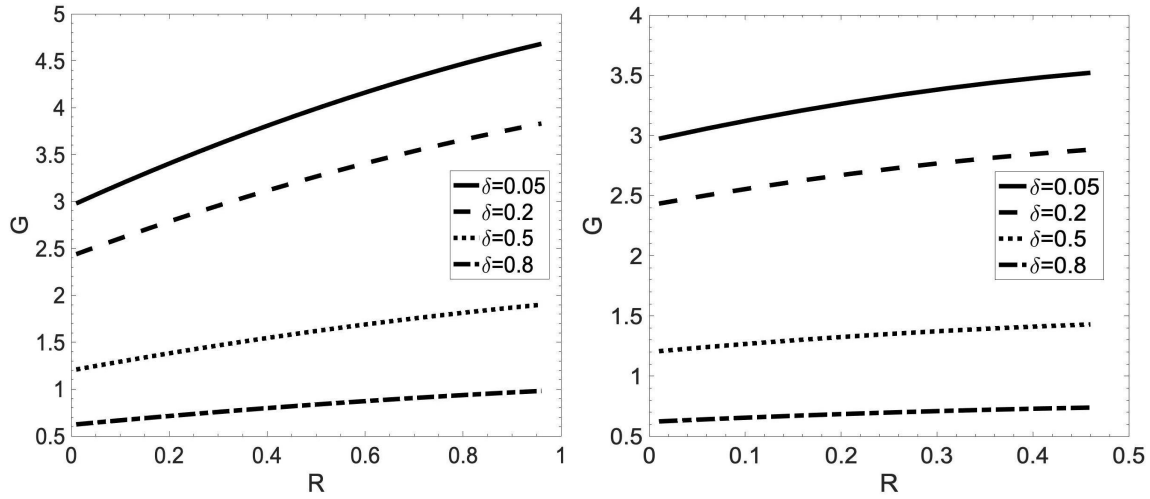

Figure 3: *On the left, plot of the neutral stability contour (3.8) in the* (R, G)*-plane with* $\mu = 0.2$ *and* $\overline{z}_v = +0.2\ell$ *for* $\delta = 0.05, 0.2, 0.5$ *and* 0.8*. On the right, plot of the neutral stability contour (3.8) in the* (R, G)*-plane with* $\mu = 0.4$ *and* $\overline{z}_v = +0.4\ell$ *for* $\delta = 0.05, 0.2, 0.5$ *and* 0.8*. Above the contour the solutions are unstable, while below the contour the solutions are stable.*

$\overline{\boldsymbol{x}}_v$ is placed at $(\mu = 0)$ or below the pivot point with the $-$ sign and when $\overline{\boldsymbol{x}}_v$ is placed

above the pivot point with the + sign, and write $D(s) = 0$ in the following form:

$$\left.\begin{aligned}&\left(-\frac{1}{12}s^2+\frac{1}{3}\delta^2 s^2+\frac{1}{8}+\frac{1}{24\delta^2}-\sigma_1^n\right)G^2\\&+\left(-\frac{1}{4}(1+R)s^2-\frac{1}{16\delta^2}(1+R)(1\pm\mu R)-\sigma_2^n\right)G\\&+\frac{1}{16\delta^2}(1+R)^2\left(1+\mu^2R\right)s^2+\sigma_3^n=0\,,\end{aligned}\right\}\tag{6.1}$$

where

$$\begin{cases}\sigma_1^n=\displaystyle\sum_{n=0}^{\infty}\left[\frac{2}{\gamma_n^3\left(\gamma_nT_n-4\delta s^2\right)}\left(\frac{16s^2}{\delta\gamma_nC_n}+\frac{T_n}{\delta^2}-16s^4\delta^2T_n+\frac{32\delta s^4}{\gamma_n}\left(1-\frac{2}{C_n}\right)\right.\right.\\\qquad\qquad\left.\left.-\frac{24s^2}{\delta\gamma_n}+\frac{64s^4}{\gamma_n^2}T_n\right)\right],\\\sigma_2^n=\displaystyle\sum_{n=0}^{\infty}\left[\frac{2}{\gamma_n^3\left(\gamma_nT_n-4\delta s^2\right)}\left(\frac{2}{\delta^2}(1+R)s^2T_n+8s^4(1+R)T_n\right.\right.\\\qquad\qquad\left.\left.+\frac{16s^4}{\delta\gamma_n}(1+R)\left(\frac{1}{C_n}-1\right)\right)\right],\\\sigma_3^n=\displaystyle\sum_{n=0}^{\infty}\left[\frac{2T_ns^4}{\delta^2\gamma_n^3\left(\gamma_nT_n-4\delta s^2\right)}(1+R)^2\right].\end{cases}$$

For each fixed R, G, δ and μ, it is a straightforward numerical calculation to plot $D(s)$ as a function of s. The only numerical difficulty is avoiding the singularity that occurs for each n at

$$s^2=\frac{(2n+1)\pi}{4\delta}\tanh\left((2n+1)\pi\delta\right)\,.\tag{6.2}$$

The terms in the sum in (6.1) are evaluated and summed. The numerical results retain 200 terms in the summation. To compute the natural frequency of the coupled pendulum-slosh system, as an example set the length, L, and width of the container to be $1\,m$ and take $\mu=0.20$ and so $\overline{z}_v=-0.2\ell$ relative to the pivot point. Set $R=0.20$, and the fluid depth $h_0=0.5\,m$, which means $m_f=500\,kg$ and $\delta=0.5$. The neutral stability values of G and ℓ calculated in (3.6) and (3.7) are $G_{st}=1.4976$ and $\ell_{st}=0.4006\,m$. Hence, it is required that $G<G_{st}$ and $\ell>\ell_{st}$. Now, set $\ell=\ell_{st}+0.05=0.4506\,m$ and so $G=1.3314<G_{st}$. With these input parameters, and using Newton's method to find the real roots of the nonlinear equation (6.1), the fundamental mode is $s=1.0188$. The numerical calculations presented in Table 1 show that as the value of G increases, i.e. as the length of the pendulum ℓ decreases, the frequency of the coupled pendulum-slosh system increases and reaches a maximum value before decreasing towards the instability contour. The angular frequency of the dry container modelled as a point mass is $\omega=\sqrt{g/(\mu\ell)}$ with $0<\mu\leq 1$, and therefore the non-dimensional frequency is

$$s_p=\sqrt{\frac{G}{\mu(1+R)}}\,,\tag{6.3}$$

which is reported in Table 1 for this numerical experiment.

The numerical evaluation of the characteristic equation (2.29) with the same input parameters reported in Table 1, and so the same values of δ and R, but with $\mu=1$ and

$\ell\,(m)$	$\ell_{st}+0.02$ $=0.4206$	$\ell_{st}+0.05$ $=0.4506$	$\ell_{st}+0.1$ $=0.5006$	$\ell_{st}+0.3$ $=0.7006$	$\ell_{st}+0.5$ $=0.9006$	$\ell_{st}+1.0$ $=1.4006$	$\ell_{st}+1.5$ $=1.9006$
G	1.4264	1.3314	1.1985	0.8564	0.6662	0.4284	0.3157
s	0.6701	1.0188	1.0981	0.9611	0.8432	0.6583	0.5548
s_p	2.4379	2.3553	2.2346	1.8890	1.6661	1.3360	1.1469

Table 1: *Numerical evaluation of the characteristic equation (2.29) for the fundamental mode $s = s_1$. The fluid density is $\rho = 1000\,kg/m^3$, and the tank length is $L = 1.0\,m$ with $h_0 = 0.5\,m$, $\mu = 0.20$, $\overline{z}_v = -0.2\ell$, $R = 0.20$, $m_f = 500\,kg$, $\delta = 0.5$, $G_{st} = 1.4976$, and $\ell_{st} = 0.4006\,m$.*

$\overline{z}_v = -\ell$ relative to the pivot point, i.e. when the centre of mass of the dry container is fixed at the centre of the base of the container, is presented in Table 2. The computed results in Table 2 show that, when $\overline{z}_v$ is placed at the base of the container, for small values of G the coupled fluid-body frequency s is very close to the dry pendulum frequency s_p and hence the tank motion is independent of the fluid motion. However, beyond some critical value of G or ℓ where the fundamental mode $s = s_1$ reaches its maximum value, the fluid motion becomes significant in determining the coupled fluid-body frequency and the coupled frequency decreases.

$\ell\,(m)$	$\ell_{st}+0.02$ $=0.3672$	$\ell_{st}+0.05$ $=0.3972$	$\ell_{st}+0.1$ $=0.4472$	$\ell_{st}+0.3$ $=0.6472$	$\ell_{st}+0.5$ $=0.8472$	$\ell_{st}+1.0$ $=1.3472$	$\ell_{st}+1.5$ $=1.8472$
G	1.6339	1.5105	1.3416	0.9270	0.7082	0.4454	0.3248
s	0.4828	0.7456	0.9763	0.9546	0.8360	0.6504	0.5474
s_p	1.1669	1.1219	1.0574	0.8789	0.7682	0.6092	0.5203

Table 2: *Numerical evaluation of the characteristic equation (2.29) for the fundamental mode $s = s_1$. The fluid density is $\rho = 1000\,kg/m^3$, and the tank length is $L = 1.0\,m$ with $h_0 = 0.5\,m$, $\mu = 1.0$, $\overline{z}_v = -\ell$, $R = 0.20$, $m_f = 500\,kg$, $\delta = 0.5$, $G_{st} = 1.7280$, and $\ell_{st} = 0.3472\,m$.*

In comparison with Table 2, the computed results in Table 1 show that when $\overline{z}_v$ is placed closer to the pivot point, i.e. for smaller values of μ, the fluid motion is significant in determining the coupled fluid-body frequency even for small values of G.

The free surface profile can be calculated from the kinematic free surface boundary condition in (2.2). Differentiating $\widehat{\Phi}(x,y)$ in (2.6) with respect to z and substituting into the kinematic boundary condition gives

$$\left\{\begin{array}{rcl} \widehat{h}(x) & = & -2\widehat{\theta}\left(x-\dfrac{L}{2}\right) \\ & & +\displaystyle\sum_{n=0}^{\infty}\left[\frac{4\widehat{\theta}}{L\alpha_n\left(g\alpha_n T_n-\omega^2\right)}\left(\frac{2\omega^2}{C_n\alpha_n}-T_n\left(g-\omega^2\left(h_0-\ell\right)\right)\right)\cos\alpha_n x\right], \end{array}\right. \tag{6.4}$$

and therefore the free surface profile can be obtained from

$$h(x,t) = h_0 + \widehat{h}(x)\cos\omega t\,. \tag{6.5}$$

Take the initial conditions $\theta(0) = \widehat{\theta}$ and $h(x,0) = h_0 + \widehat{h}(x)$, set $\overline{z}_v = -0.1\ell$ relative to

the body frame $\overline{\boldsymbol{x}}_v$ at the pivot point, and set the input parameters

$$\begin{cases} \widehat{\theta} = 0.1745\, rad\,, \quad L = 1\, m\,, \quad h_0 = 0.4\, m\,, \quad \rho = 1000\, kg/m^3\,, \\ g = 9.81\, m/s^2\,, \quad m_f = 400\, kg\,, \quad \delta = 0.4\,, \quad R = 0.4\,, \quad \mu = 0.1\,, \\ \ell_{st} = 0.3926\, m\,, \quad \ell = 0.6426\, m\,, \quad G_{st} = 2.2286\,, \quad G = 1.3616\,. \end{cases} \tag{6.6}$$

The panel on the left in Figure 4 shows the plot of the wave profile $h\,(x,t)$ in (6.5) at three different times $t = 0.0\, s$, $t = 0.5T = 0.74\, s$ and $t = 0.2T = 0.29\, s$, where $T = 2\pi/\omega = 1.48\, s$, for the fundamental mode $s = s_1 = 1.0669$. The numerical results retain 200 terms in the summation in (6.4). Snapshots of the free surface profile show that the tank and water motions are in *phase*: as the tank swings to the left, the waterline at the left-hand end of the tank rises until maximum run-up coincides with the time of extreme displacement of the tank to the left. The wave profile resembles a standing wave with one node for the first root of the characteristic function.

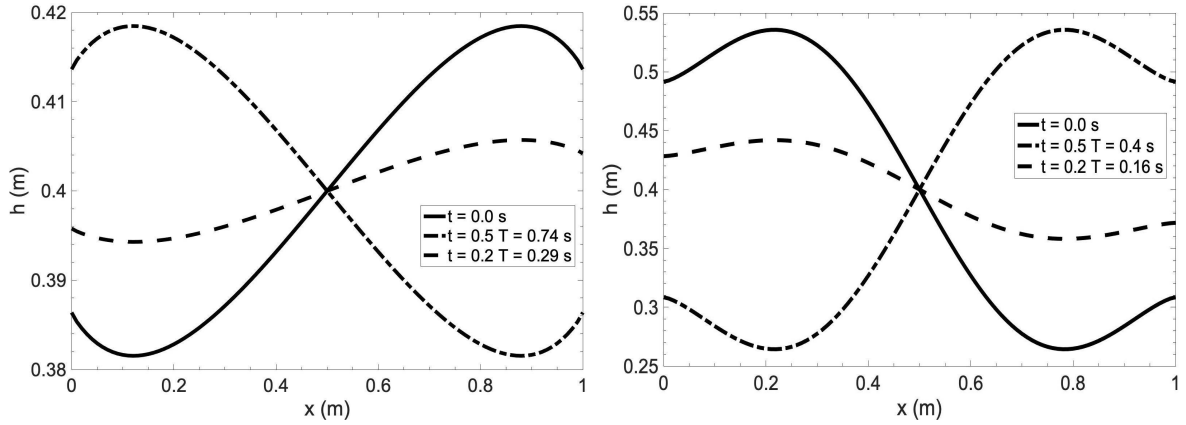

Figure 4: *On the left, plot of* $h\,(x,t)$ *with* $\delta = 0.4$, $R = 0.4$, $G = 1.3616$, $\mu = 0.1$, $\overline{z}_v = -0.1\ell$ *relative to the pivot point, and* $s = s_1 = 1.0669 < s_0^{(a)} = 1.2919$. *The surface oscillates in phase with the pendulum. On the right, plot of* $h\,(x,t)$ *with the same input parameters, but with* $s_0^{(a)} < s = s_2 = 1.9719 < s_1^{(a)}$. *The surface oscillates in antiphase with the pendulum.*

One interesting feature of this experimental system occurs close to the frequencies of the free anti-symmetric sloshing modes, which occur with the non-dimensional frequencies:

$$s_n^{(a)} = \frac{1}{2}\,(2n+1)\,\pi\sqrt{\frac{\tanh\left((2n+1)\,\pi\delta\right)}{(2n+1)\,\pi\delta}}\,, \quad n = 0, 1, 2, \ldots\,,$$

which is the singular frequency (6.2) for each n in the characteristic function (2.29). Using the same input parameters (6.6) of the previous numerical experiment, we have $s_0^{(a)} = 1.2919 > s_1 = 1.0669$, and the second root of the characteristic function $D(s) = 0$ is $s_0^{(a)} < s = s_2 = 1.9719 < s_1^{(a)} = 2.4257$. Now, using the initial conditions $\theta\,(0) = \widehat{\theta}$ and $h\,(x,0) = h_0 + \widehat{h}\,(x)$, the plot of the wave profile $h\,(x,t)$ at three different times $t = 0.0\, s$, $t = 0.5T = 0.4\, s$ and $t = 0.2T = 0.16\, s$, where $T = 0.8\, s$, is illustrated on the right in Figure 4. Snapshots of the free surface profile show that the tank and water motions are

in *antiphase*: as the tank swings to the left, the waterline at the right-hand end of the tank rises until maximum run-up coincides with the time of extreme displacement of the tank to the left.

6.2 Results at 1:1 resonance

The next simulation is devoted to the coupled pendulum-slosh oscillations at $1:1$ resonance in the finite depth. In TAAB (2015) the centre of mass of the dry container is fixed at the base of the container along the centre line, and so the $1:1$ resonance in the finite depth was unlikely to be observed for an experimentally realistic setup and in particular for $0 < R < 1$. However, in our analysis in the current paper, with the new quadratic equation (5.3) for G including the parameter μ, the $1:1$ resonance in the finite depth can be observed for an experimentally realistic setup and even for $0 < R < 1$. This is because the condition in TAAB (2015) on the centre of mass of the dry container is relaxed and so $\overline{z}_v$ is placed above the base of the container along the centre line, i.e. $\overline{z}_v = -\mu\ell$ with $0 < \mu < 1$ (relative to the pivot point) or $\overline{z}_v = +\mu\ell$ with $\mu \in \mathbb{R}_{>0}$. See §5 for more details.

For fixed m in (5.2) and fixed δ and μ the quadratic equation (5.3) gives a line in the (R, G)-plane along which there is a resonance. Calculations for a range of physically realisable parameter values for δ, λ, G, and R are presented in Figures 5 and 6.

Calculations for different (δ, μ) values are shown in Figure 5 for $0 < R < 1$. The panel on the left in Figure 5 shows the plot of the first $(m = 1)$ resonance curve in the (R, G)-plane for the first root G_1 of the quadratic equation (5.3) with $\overline{z}_v = -\mu\ell$ and $0 < \mu < 1$, and the panel on the right shows the first resonance curve for the second root G_2 of (5.3) with the same values for the parameters δ and μ. Note that the illustrated roots G_1 and G_2 in Figure 5 satisfy the stability condition (5.5).

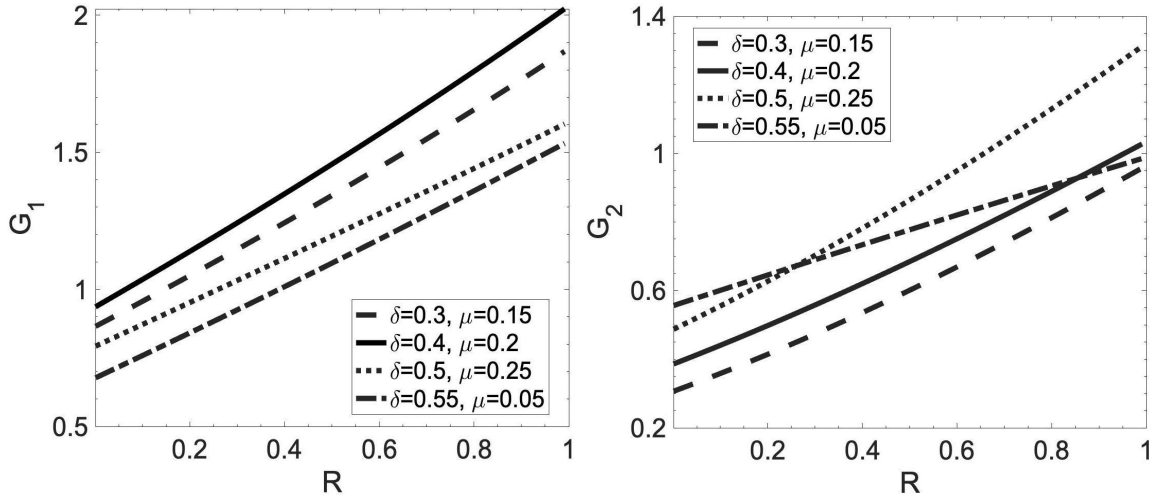

Figure 5: *On the left, plot of the first* $(m = 1)$ *physically realisable resonance curve in the* (R, G)*-plane for the first root* G_1 *of the quadratic equation (5.3), with* $\overline{z}_v = -\mu\ell$*, for a range of* δ *and* μ *values:* $(\delta, \mu) = (0.3, 0.15)$*,* $(\delta, \mu) = (0.4, 0.2)$*,* $(\delta, \mu) = (0.5, 0.25)$ *and* $(\delta, \mu) = (0.55, 0.05)$*. On the right, plot of the first* $(m = 1)$ *physically realisable resonance curve in the* (R, G)*-plane for the second root* G_2 *of (5.3), with* $\overline{z}_v = -\mu\ell$*, and the same set of* (δ, μ) parameter values.

As δ is increased, the $1:1$ resonance between the symmetric sloshing modes and

the anti-symmetric sloshing modes and the pendulum motion can be observed for larger values of R. The first $(m = 1)$ resonance curves, in the (R, G)-plane, for the roots G_1 and G_2 of the quadratic equation (5.3) for $(\delta, \mu) = (0.6, 0.1)$ and $0.6 < R < 1.2$ are illustrated on the left panel in Figure 6. Also the first resonance curves, in the (R, G)-plane, for the

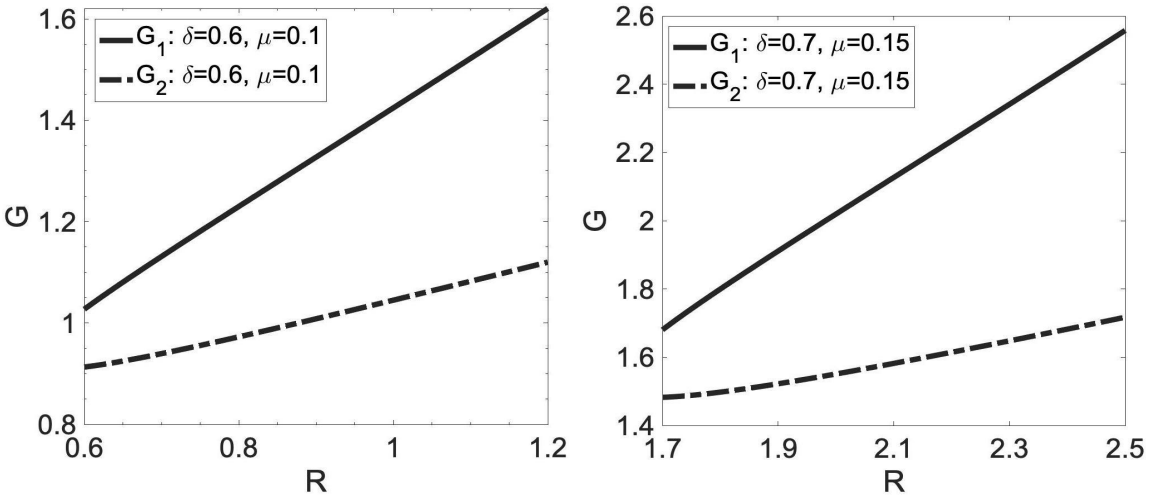

Figure 6: *On the left, plot of the first* $(m = 1)$ *physically realisable resonance curves in the* (R, G)*-plane for the first and the second roots* G_1 *and* G_2 *of the quadratic equation (5.3), with* $\overline{z}_v = -\mu\ell$*, for* $(\delta, \mu) = (0.6, 0.1)$*. On the right, plot of the first* $(m = 1)$ *physically realisable resonance curves in the* (R, G)*-plane for the first and the second roots* G_1 *and* G_2 *of (5.3), with* $\overline{z}_v = -\mu\ell$*, for* $(\delta, \mu) = (0.7, 0.15)$.

roots G_1 and G_2 of (5.3) or $(\delta, \mu) = (0.7, 0.15)$ and $1.7 < R < 2.5$ are illustrated on the right panel in Figure 6. The resonance curves in Figure 6 satisfy the stability condition (5.5).

Next, for an experimentally realistic numerical experiment at $1:1$ resonance, set the container length $L = 1\,m$, $R = 0.2$, $\mu = 0.25$ with $\overline{z}_v = -0.25\ell$ relative to the origin of the body frame $\overline{\boldsymbol{x}}_v$ placed at the pivot point. Set the initial fluid depth $h_0 = 0.5\,m$ and so $\delta = 0.5$. For the first resonance mode set $m = 1$ in (5.2) and so $s_1 = 1.7691$. With the given input parameters, there are two positive real roots of the quadratic equation (5.3) for G at $1:1$ resonance, which are $G_1 = 0.9519 < G_{st} = 1.5120$ and $G_2 = 0.6274 < G_{st}$. Hence, from the dimensionless variable G in (2.24), it can be concluded that the $1:1$ resonance occurs when the length of the pendulum is $\ell_1 = 0.6303\,m$ or $\ell_2 = 0.9564\,m$ which correspond to G_1 and G_2, respectively. Note that the resonance values for ℓ_1 and ℓ_2 satisfy the stability condition $\ell_1 > \ell_{st} = 0.3968\,m$ and $\ell_2 > \ell_{st}$. The free surface mode shapes at $1:1$ resonance take the form

$$\left\{\begin{array}{rcl} \widehat{h}\,(x) & = & -2\widehat{\theta}\,(x - (L/2)) - \dfrac{1}{\omega_m} b_m \beta_m \widehat{S}_m \cos\beta_m x \\ & & + \displaystyle\sum_{n=0}^{\infty} \left[\frac{4\widehat{\theta}}{L\alpha_n\,(g\alpha_n T_n - \omega_m^2)} \left(\frac{2\omega_m^2}{C_n\alpha_n} - T_n\left(g - \omega_m^2\,(h_0 - \ell_{1,2})\right) \right) \cos\alpha_n x \right] \end{array}\right. \tag{6.7}$$

where $\widehat{S}_m = \sinh(\beta_m h_0)$ and $\omega_m = \left(2\sqrt{g h_0}/L\right) s_m$, and the two parameters b_m and $\widehat{\theta}$ are arbitrary. For this simulation the first $(m = 1)$ resonance frequency is $\omega_1 = 7.8363\,rad/s$ and so $T_1 = 2\pi/\omega_1 = 0.8018$. Take $G = G_2$ and $\ell = \ell_2$ which means $d_3 = -\ell_2$ in

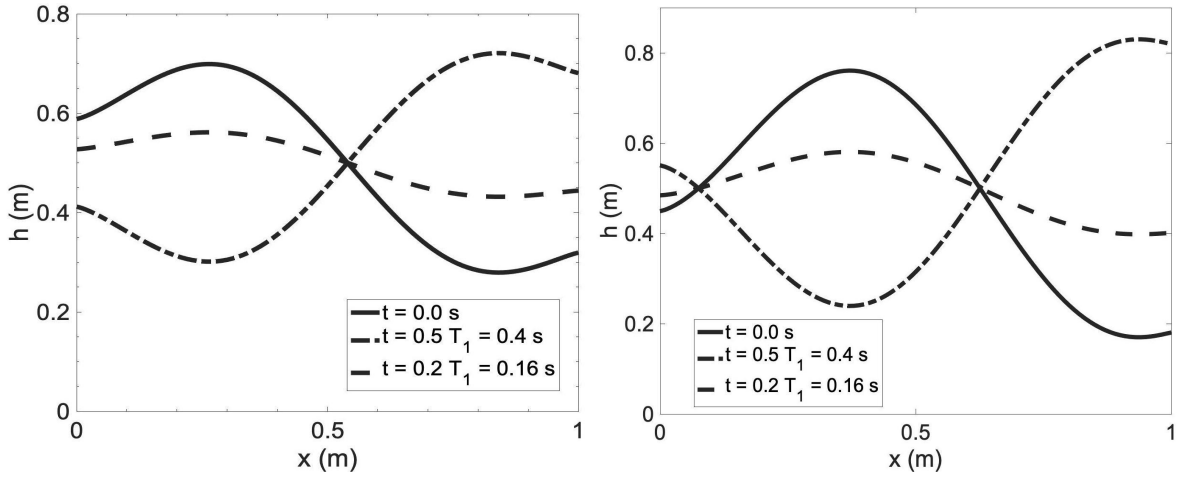

Figure 7: *On the left, plot of* $h(x,t)$ *for the first* $(m=1)$ $1:1$ *resonance mode with* $\delta = 0.5$, $R = 0.2$, $G_2 = 0.6274$, $\mu = 0.25$, $\overline{z}_v = -0.25\ell_2$ *relative to the pivot point, where* $\ell_2 = 0.9564\,m = d_3$, *and* $b_1 = 0.005$ *in (6.7). The surface oscillates in antiphase with the pendulum. On the right, plot of* $h(x,t)$ *at* $1:1$ *resonance with the same input parameters* δ, R, G_2, μ, ℓ_2, m, *but with* $b_1 = 0.02$. *The wave profile resembles a standing wave with two nodes which oscillates in antiphase with the pendulum.*

(6.7), and set $b_1 = 0.005$ and $\widehat{\theta} = 0.1396\,rad$. Take the initial conditions $\theta(0) = \widehat{\theta}$ and $h(x,0) = h_0 + \widehat{h}(x)$. Snapshots of the free surface profile at $1:1$ resonance, with $m = 1$, at $t = 0\,s$, $t = 0.2T_1 = 0.16\,s$ and $t = 0.5T_1 = 0.4\,s$ are shown on the left in Figure 7. The wave profile resembles a standing wave with one node which oscillates in antiphase with the pendulum. The numerical results retain 200 terms in the summation in (6.7). Snapshots of the free surface profile at $1:1$ resonance with the same input parameters δ, R, G_2, μ, ℓ_2, m, but with $b_1 = 0.02$ are shown on the right in Figure 7. The wave profile resembles a standing wave with two nodes which oscillates in antiphase with the pendulum.

The internal resonances are of interest because symmetric sloshing modes are dynamically coupled to the anti-symmetric sloshing modes, and hence the pendulum motion. Such resonances are pathways for energy exchange within fluid modes. Turner and Bridges (2013) showed that for Cooker's pendulous sloshing experiment, there is a single fluid height where there exists a heteroclinic orbit between the purely symmetric and purely anti-symmetric modes. Solutions close to this heteroclinic orbit can manifest themselves in an experiment by having an oscillating container slowly coming to rest as the energy is transferred from the vessel to the symmetric modes or a stationary vessel containing a symmetric sloshing mode starting to oscillate as the energy is transferred to the anti-symmetric modes, and hence the vessel.

7 Concluding remarks

In this paper, we first showed the usefulness of the two-dimensional variant of the Bateman–Luke variational principle presented in Alemi Ardakani (2020) for the problem of dynamic coupling between a rigid body and its interior potential fluid sloshing. Then, the Euler-Lagrange equations emerging from this variational principle are linearised about the state

of quiescent fluid and analytical solutions are presented. We found that the coupled pendulum-slosh system exhibits unstable solutions if the length of the rigid rod is less than some critical value which is defined in (3.7). The instability transition is associated with the potential emergence of homoclinic behaviour in the nonlinear coupled system.

In the case of stable solutions there is a $1:1$ resonance between the symmetric sloshing modes and the anti-symmetric sloshing modes, and hence the rigid body motion. The presented numerical calculations show that internal $1:1$ resonances can be observed, for a range of values of the dimensionless variables δ, G, R, and λ (and so μ), for experimentally realistic setups.

The pendulum-sloshing problem provides a simplified model for the slosh-induced rolling of a ship. It is also useful as a model for the mathematical modelling of floating ducted wave energy converters where the two-dimensional translational motion of the pivot point can be added to the coupled fluid-body equations. Constructing a weakly nonlinear analysis about the $1:1$ resonances would show whether heteroclinic orbits exists between the symmetric and anti-symmetric sloshing modes which are pathways for energy exchange within fluid modes, and of prime importance for modelling the power take off system in wave energy converters.

Acknowledgements

The work of HAA & TJB is supported by the EPSRC under grant number EP/W033062/1. The work of MRT is supported by the EPSRC under grant number EP/W006545/1. For the purpose of open access, the authors have applied a Creative Commons Attribution (CC BY) licence to any Author Accepted Manuscript version arising.

References

[1] H. Alemi Ardakani, An alternative view on the Bateman–Luke variational principle, Euro. J. Mech. B/Fluids 82 (2020) 39–46.

[2] H. Alemi Ardakani, T.J. Bridges, M.R. Turner, Resonance in a model for Cooker's sloshing experiment, Euro. J. Mech. B/Fluids 36 (2012) 25–38.

[3] M.J. Cooker, Water waves in a suspended container, Wave Motion 20 (1994) 385–395.

[4] O.M. Faltinsen, A.N. Timokha, Sloshing, Cambridge University Press, Cambridge, 2009.

[5] J.B. Frandsen, Numerical predictions of tuned liquid tank structural systems, J. Fluids Struct. 20 (2005) 309–329.

[6] R.A. Ibrahim, Liquid Sloshing Dynamics, Cambridge University Press, Cambridge, 2005.

[7] I.A. Lukovsky, Nonlinear Dynamics: Mathematical Models for Rigid Bodies with a Liquid, De Gruyter, Berlin, 2015.

[8] N.N. Moiseyev, V.V. Rumyantsev, Dynamic Stability of Bodies Containing Fluid, Springer-Verlag, New York, 1968.

[9] M.R. Turner, H. Alemi Ardakani, T.J. Bridges, Instability of sloshing motion in a vessel undergoing pivoted oscillations, J. Fluids Struct. 52 (2015) 166–180.

[10] M.R. Turner, T.J. Bridges, Nonlinear energy transfer between fluid sloshing and vessel dynamics, J. Fluid Mech. 719 (2013) 606–636.